



# Retrospective computed tomography assessment of chemotherapy-related pneumonia with severity screening in pediatric acute lymphoblastic leukemia by radiological imaging

Zhixin Gao<sup>a,b</sup>, Ke Wei<sup>c</sup>, Ruiyuan Chen<sup>a,b</sup>, Wenhong Ye<sup>a</sup>, Tian Li<sup>d</sup>, Qiru Su<sup>e</sup>, Rong Wang<sup>f</sup>, Weiguo Cao<sup>a,\*</sup>

<sup>a</sup> Department of Radiology, Shenzhen Children's Hospital, 7019 Yitian Road, Futian District, Shenzhen, China

<sup>b</sup> China Medical University, No.77 Puhe Road, Shenbei New District, Shenyang, China

<sup>c</sup> Department of Radiology, Guangdong Provincial Hospital of Traditional Chinese Medicine, Guangzhou, Guangdong Province, China

<sup>d</sup> Department of Pathology and Cell Biology, Columbia University Medical Center, New York, NY, USA

<sup>e</sup> Institute of Pediatrics, Shenzhen Children's Hospital, 7019 Yitian Road, Futian District, Shenzhen, China

<sup>f</sup> Department of Neurology, Zhongshan Hospital Xiamen University, Xiamen, China

## ARTICLE INFO

### Keywords:

Pediatric  
Acute lymphoblastic leukemia  
Chest computed tomography  
Pneumonia  
Severity

## ABSTRACT

**Objectives:** To evaluate the radiological imaging-guided severity along the pneumonia course and evaluate the chest computed tomography (CT) findings of chemotherapy-related pneumonia in children with acute lymphoblastic leukemia (ALL).

**Materials and methods:** A retrospective database review of children with ALL was conducted from March 2016 to August 2021 to identify cases with CT images who developed pneumonia during the chemotherapy course. A total of 51 children with ALL developed pneumonia were ultimately included (31 boys and 20 girls, mean age:  $6 \pm 4$  years [standard deviation]). Each child's demographics, medical records, and laboratory results were collected. The CT images were then reviewed and the radiologic severity index (RSI) was calculated based on the regional opacity and implicated volume. A *t*-test, *U* test, Pearson's Chi-square test, and Fisher's exact test were performed to compare the clinical or radiologic features between the severe and moderate cases. The linear regression models were employed to analyze the correlation of RSIs with other clinical features.

**Results:** Eleven children (22 %, 11/51) displayed severe phenotypes associated with respiratory failure. The ground glass opacity (GGO) frequently appeared (65 % of CT images). The baseline RSI was positively associated with the lowest lymphocyte ( $p = .003$ ), neutrophil ( $p = .01$ ) counts, and the highest C-reactive protein level ( $p = .04$ ). The peak RSI may predict severe phenotypes at a cutoff of 4.5 (AUC 0.76 [0.61, 0.91]) with 73 % sensitivity and 63 % specificity.

**Conclusion:** The chest CT images of children with chemotherapy-related pneumonia displayed clinically related baseline RSI and a peak RSI of  $>4.5$  of 36 predicted severe phenotypes.

\* Corresponding author.

E-mail address: [weiguo.cao@126.com](mailto:weiguo.cao@126.com) (W. Cao).

<https://doi.org/10.1016/j.heliyon.2023.e23444>

Received 19 July 2023; Received in revised form 2 December 2023; Accepted 4 December 2023

Available online 9 December 2023

2405-8440/© 2023 Published by Elsevier Ltd.

This is an open access article under the CC BY-NC-ND license

(<http://creativecommons.org/licenses/by-nc-nd/4.0/>).

## 1. Introduction

### Abbreviations

ALL	acute lymphoblastic leukemia;
RSI	radiologic severity index
TRM	treatment-related mortality
GGO	ground-glass opacity
PICU	pediatric intensive care unit
WBC	white blood cell or leukocyte
CRPC	reactive protein
ROC	C reactive protein
ROC	receiver operating characteristic
AUC	area under the curve
CXRs	chest radiographs
COVID-19	coronavirus disease 2019
HAP	hospital-acquired pneumonia
ICUs	intensive care units
VAP	ventilation-associated pneumonia

The therapeutic strategies for pediatric acute lymphoblastic leukemia (ALL), the highest-incidence childhood malignancy [1], have dramatically improved the overall survival rate of ALL children over the past two decades [2]. Treatment-related toxicity, on the other hand, has been a widespread concern in oncology clinical practice [3,4], albeit that has been relatively less studied when compared to the positive effects of treatments on the survival rate. Treatment-related mortality (TRM) has recently been reported in child ALL-treatment clinical trials, ranging from 2 % to 5 % [5]. Infection is the most prevalent cause of TRM [6], and infection-related mortality (IRM) accounts for 64–73 % of all TRM cases [6–10], possibly due to the predominantly immunosuppressive effect of chemotherapy regimens. The evidence of infection sites revealed that 29–35 % of infections were respiratory, which is a higher ratio than the bloodstream [11], gastrointestinal, and central nervous system infections [6].

Owing to its high sensitivity for early identification [12] and non-invasive nature to aid patients with severe bleeding and increased infection risks [13], chest CT imaging is a standard procedure for the diagnosis and severity evaluation of respiratory infection. The chest CT scan can also be rapidly applied for suspected cases with respiratory symptoms [14]. The severity of SARS-Cov2 infection [15–17] and influenza H7N9 pneumonia [18] has been evaluated using semi-quantitative visual analysis of lung attenuation. The CT severity of SARS-CoV2 infection was further categorized into three grades based on the severity score (full 25 points), as follows: mild (<8/25), moderate (9–15/25), and severe (>15/25). The severe (>15/25) groups had significantly higher levels of inflammatory markers, such as CRP and leukocytosis, when compared to the other two groups [17]. Another SARS-COV2 infection study revealed that CT severity scores >18 (of 25) were associated with an increased mortality risk and could predict death in short-term follow-up [19].

In adult patients with acute leukemia, the severity score (radiologic severity index, RSI) was also used to assess treatment-related pulmonary infection [20]. The study found that each one-point increase in RSI was associated with a 7 % increase in mortality within 33 days. The highest (peak) RSI during pneumonia was associated with increased treatment costs, more time spent in the intensive care unit, and a greater possibility of requiring mechanical ventilation [20]. The goal of this study was to assess the RSI of chemotherapy-related pneumonia in ALL children and provide novel evidence for future studies and clinical practice.

## 2. Materials and Methods

The Research Ethics Committee at Shenzhen Children's Hospital in China accepted the retrospective collection and assessment of research subjects' demographic, clinical, and radiologic data. Under the research protocol, we also obtained the waiver of informed written consent for the patients and guardians (Protocol number JCYJ20220530155607018).

### 2.1. Patients

From March 2016 to August 2021, 295 children were diagnosed with ALL for the first time at Shenzhen Children's Hospital. Of them, 139 ALL children were treated with risk-based chemotherapy regimens of South China children's leukemia Group (SCCLG-ALL-2016, CCCG-ALL-2020) without delay by complications. The inclusion criteria were established by the diagnosis of clinical and pathological evidence of ALL, as well as the availability of complete medical history records, clinical test results, treatment, and radiological exams. The exclusion criteria included being partially or previously treated with chemotherapy before moving to our center, systematic glucocorticoid usage a month before the chemotherapy schedule, any specific treatment before chemotherapy due to infection or other complications, interruption of chemotherapy due to non-compliance, diagnosis of mature B-cell ALL, mixed phenotype leukemia, secondary malignancy, chronic myeloid leukemia acute phase, accompanying immunodeficiency, or prior lung diseases with remaining radiological signs. The research team carefully reviewed the demographics, chemotherapy and pneumonia

clinical data, pathology results, and clinical test results of the selected ALL children. The entire chemotherapy process of 139 ALL children was then reviewed. From the first diagnostic confirmatory CT until 3 months following the onset of pneumonia, clinical and radiologic data from 51 children were obtained (31 boys and 20 girls, mean age:  $6 \pm 4$  years [standard deviation]). The clinical data collected from the institutional database included the leukocyte count (baseline) on the day the first chest CT confirmed the diagnosis of chemotherapy-related pneumonia, the lowest counts of hematocytes (i.e., lymphocytes, neutrophils, erythrocytes, or platelets), and the liver panel (i.e., albumin, globulin, or C-reactive protein [CRP]) throughout pneumonia. ALL children with major clinical manifestations or respiratory failure treated in the pediatric critical care unit (PICU) with respiratory assistance or ventilation were considered "severe cases". The "moderate cases" had less intense clinical progress and were managed in the pediatric unit without ventilation.

## 2.2. CT protocol

The GE optima680 64-row CT scanner was utilized with patients in the supine position to scan from the lung apex to the lung base. Scanning parameters: Detector collimation width of 40 mm, layer thickness of 5 mm ( $\leq 3$  years old, 3–7 years old) and 7.5 mm ( $\geq 7$  years old), spiral pitch of 0.984/1, speed of 0.5s, tube voltage of 100–120 kV with automatic tube current modulation, matrix of  $512 \times 512$ , FOV of 200–350. Standard algorithm reconstruction was employed, with a reconstructed slice thickness of 1.25 mm (lung window: window width 1000 HU, window level  $-500$  HU; Mediastinal window: Window width 350 HU, window position 40 HU). For non-cooperative pediatric patients, sedation was administered using chloral hydrate at a dose of 2 mL/kg, not exceeding a maximum of 10 ml.

The median CTDIvol (DLP) was 2.57 mGy (60.01 mGy cm).

## 2.3. Radiologic evaluation and severity score

Thin-section CT scans were reviewed independently by two experienced radiologists (CWG and YWH, with 19 and 15 years of experience in chest imaging, respectively) with blinded patient identification and clinical information. The final decisions of diagnosis and severity were determined by consensus. With reference to the Fleischner Society Thoracic Imaging Glossary [21], the images of ALL children with pneumonia symptoms were evaluated for the presence of the following findings: ground-glass opacity (GGO—a slight increase in attenuation without concealing underlying vessels and airway walls), consolidation (dense opacification with obscured broncho vascular margins), nodules (small rounded opacities), interstitial thickening, airway signs (stagnation, airway dilatation, or tree-bud sign), and the extrapulmonary lesions (pleural effusion or thoracic lymphadenopathy). The RSI score was calculated by multiplying the opacity (GGO or consolidation) and the involved percentage of six zones (i.e., bilateral upper, middle, or lower zones) [20]. A GGO was worth one point, whereas a dense cluster of nodules was worth two points. The percent areas were defined as zero points for no opacity change in one zone, one point for 1–24 % opacity area, two points for 25–50 %, three points for 51–75 % area, and four points for  $>76$  % area involved. The final RSI was calculated by adding the scores from six zones, which varied from 0 to 36. The baseline RSI was the score of confirmatory chest CT for pneumonia. The peak RSI was the highest RSI score during pneumonia treatment. The delta RSI represented the difference between the baseline and peak RSI values. The RSI varying rate was defined as the ratio of score increment from baseline RSI to peak RSI and the interval (days).

A four-point visual grading system (VGS) based on comparisons of the brightness of the liver with those of hepatic vessels on unenhanced CT images was developed as follows: grade 0 (G0; hepatic vessels showing lower attenuation than the hepatic parenchyma, with no or minimal margin blurring in less than one-third of the liver), grade 1 (G1; hepatic vessels showing lower attenuation than hepatic parenchyma but with margin blurring in more than one-third of the liver), grade 2 (G2; hepatic vessels showing the same attenuation as hepatic parenchyma), and grade 3 (G3; hepatic vessels showing higher attenuation than hepatic parenchyma) [22,23].

## 2.4. Statistical analysis

The mean  $\pm$  standard deviation (SD) or median (interquartile spacing) for continuous variables and case number (percent) for dichotomous variables were applied to summarize patient demographic and clinical test data. The statistical software SPSS26.0 (IBM, Armonk, NY, USA) was used to examine the group comparison (both severe and moderate cases), with Student's *t*-test or Mann–Whitney *U* test for continuous data and Pearson  $\chi^2$  test or Fisher's exact test for categorical data. The binary logistic regression models using Prism (GraphPad, Boston MA, USA) were built to associate predictor variables with "severe case" phenotype, calculate the area under the receiver operating characteristic (ROC) curve, and define the optimal cutoff as the value with the maximum sum of sensitivity and specificity. Multivariate logistic regression models correlated the RSI scores and clinical test data, and  $p < .05$  was set to reach statistical significance. The intraclass correlation (ICC) was calculated to evaluate the consensus between two radiologists.

## 3. Results

### 3.1. Patient characteristics

A total of 139 ALL children without prior pulmonary infection before chemotherapy were pre-selected. The study comprised 51 (51/139, 37 %) subjects who developed pneumonia after undergoing chemotherapy (31 boys and 20 girls, mean age:  $6 \pm 4$  years [standard deviation]). Pneumonia struck 30 children (59 %) during induction, 3 (6 %) during consolidation, 13 (25 %) during

reinduction, 3 (6 %) during the first interphase, and 3 (6 %) during maintenance. Chemotherapy-related pneumonia occurred in 37 % of patients (51/139). Fig. 1 depicts the enrollment and case selection processes. Based on the integrated risk stratification of pediatric ALL, ten children (10/51, 20 %) were classified as standard risk (SR), 35 (69 %) as high-risk (HR), and 6 (12 %) as very high-risk (VHR). The mean time from the initiation of chemotherapy to the onset of pneumonia was 109 days (17–592 days). Few patients showed positive findings from bacterial, fungal, viral, or mixed infections. Some children suffered from productive cough and chest pain. A few developed progressive shortness of breath. The breath sound became more intense, and the scattered rales or wheezes could be heard. Respiratory depression was recorded in severe instances. Several children displayed low absolute neutrophil count (41/51, 80 %, ANC  $<0.5 \times 10^9/L$ ), anemia (27/51, 53 %, erythrocytes  $<3 \times 10^{12}/L$ ), thrombocytopenia (28/51, 55 %, platelets  $<70 \times 10^9/L$ ), and hypoalbuminemia (32/51, 63 %, serum albumin  $<35 \times 10^9/L$ ) within a certain time period. Nineteen cases (19/51, 37 %) remained in low ANC status over 7 days. Most children had normal serum globulin levels ( $>20$  g/L). Table 1 lists the demographic and clinical features of the enrolled children. Among the 51 children, 11 (22 %) required respiratory assistance in the PICU due to worsening hypoxia and respiratory distress, which were categorized as severe cases (Fig. 2), and one (2 %) died from complicated heart failure. The remaining 40 cases were defined as moderate (Fig. 3).

### 3.2. Chest CT findings of chemotherapy-related pneumonia

The pathologic involvement of alveoli (ground glass shadow, GGO), interstitia (interlobular septal thickening, interlobular line, or central lobular shadow), and airways was exhibited by pulmonary imaging results in the youngsters (such as gas retention, bronchial wall thickening, bronchiectasis, or tree bud sign). The most widespread lesions were alveolar ( $n = 33$  [65 %], peak RSI 5 [3–16]), followed by interstitial lesions ( $n = 6$  [12 %], peak RSI 2 [1–3]) and airway lesions ( $n = 7$  [14 %], peak RSI 2 [1–3]). The GGO was the most common finding (33/51, 65 %); patchy solid shadow (18/51, 35 %); and nodular shadow (15/51, 30 %) were also observed. The median number of CT exams was 5 (2–7) per case. Ten cases demonstrated a single lesion (a nodule, an area of consolidation, a lumpy area, or a GGO). The remaining cases (41/51) displayed multiple focal lesions with bilateral lung dissemination. The most prevalent observation of intra-thoracic non-pulmonary symptoms was pleural effusion (11/51, 22 %). Hepatic steatosis was also found to be associated with extra-thoracic abnormalities (23/51, 45 %). Eight of the patients had a visual grade of G2 and 15 had a grade of G3. Table 2 displays the intra-thoracic CT findings with the case number of involvement.

### 3.3. Radiologic severity evaluation and clinical relevance

Two radiologists evaluated 328 chest CT scans from 51 ALL children with RSI scores. The ICC was 0.98 (95 % CI 0.974–0.985). The “severe cases” with pneumonia received a median of 7 chest CT exams throughout the therapy duration, whereas the “moderate cases” received a median of 4. Most subjects had a baseline RSI of  $<7$  (47/51, 92 %). The peak RSI had a broader and higher score distribution than the baseline RSI (Fig. 4). Only 12 ALL children (24 %) had a positive value of delta RSI, indicating that the radiologic signs were progressing despite the treatment. The remaining cases (39/51, 77 %) maintained a peak RSI equal to the baseline RSI. The baseline RSI was positively associated with the lymphocyte counts ( $r = 0.41$ ;  $p = .003$ ) and the ANC ( $r = 0.35$ ;  $p = .01$ ) (Fig. 5). The cutoff

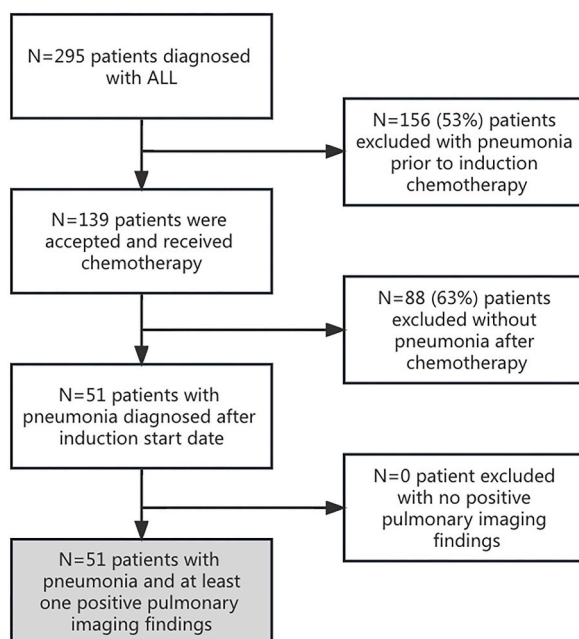


Fig. 1. The flow chart of retrospective case enrollment for chemotherapy-related pneumonia of children with acute lymphoblastic leukemia.

**Table 1**

Demographics and clinical characteristics of severe cases and moderate cases of chemotherapy-related pneumonia in children with acute lymphoblastic leukemia (ALL).

	ALL Children with chemotherapy-related pneumonia		p value
	Severe cases	Moderate cases	
Age (year)	5.5 (3.8–9.4)	4.5 (2.9–7.8)	.271
Sex(n)			
Male	8	23	.570
Female	3	17	
BMI	18.37 ± 5.46	19.01 ± 4.46	.722
Type of ALL(n)			
T lineage-ALL	1	4	1.000
B lineage-ALL	10	36	
Risk stratification (n)			
Very high risk (VHR)	1	5	.670
High risk (HR)	9	26	
Standard risk (SR)	1	9	
Fusion gene (n)			
Positive	6	17	.712
Negative	5	23	
Leukocyte (10 <sup>9</sup> /L)	0.54(0.42–1.44)	0.51(0.28–1.07)	.716
Lymphocyte (10 <sup>9</sup> /L)	0.24(0.17–0.33)	0.37(0.21–0.74)	.200
*ANC (10 <sup>9</sup> /L)	0.23(0.07–0.62)	0.05(0.02–0.32)	.245
Erythrocyte (10 <sup>12</sup> /L)	2.96 ± 0.52	4.76 ± 5.79	.327
Platelet count (10 <sup>9</sup> /L)	67.29 ± 63.56	54.59 ± 61.10	.559
Albumin (g/L)	31.8(29.3–38.2)	29.5(26.6–35.5)	.547
Globulin (g/L)	22.10 ± 3.75	21.34 ± 4.34	.571
Neutrophils lack time (d)	8.5 (2.3–23.0)	10.0(4.0–13.8)	.636
Procalcitonin (ng/mL)	0.20(0.09–1.15)	0.63(0.21–1.62)	.673

Categorical variables were shown as counts (n) and analyzed with Fisher exact test or  $\chi^2$  test. Continuous variables were described as mean ± standard deviation for normally distributed data and analyzed with a student's t-test between the severe and moderate cases. The skewed continuous data shown as median (interquartile range) was analyzed with the Mann-Whitney *U* test between two groups. \*ANC: absolute neutrophil count.

criteria for leukocyte counts were then purposefully set lower or higher than  $0.5 \times 10^9/L$  or  $1.0 \times 10^9/L$  for further investigation. When the leukocyte counts exceeded  $1.0 \times 10^9/L$  ( $n = 15$ ), the linear relationship between lymphocyte counts ( $r = 0.82, p < .001$ ) or ANC ( $r = 0.61, p < .001$ ) and baseline RSI was more vital (Fig. 4). If the leukocyte counts higher than  $0.5 \times 10^9/L$  were examined, the linear regression between lymphocyte counts ( $r = 0.76, p < .001$ ) or ANC ( $r = 0.61, p < .001$ ) and baseline RSI remained robust (Fig. 5). Another systematic marker, CRP, exhibited a similar relationship with baseline RSI, with the highest CRP levels found to be positively associated with leukocyte counts  $>0.5 \times 10^9/L$  ( $r = 0.47, p = .03$ ) or  $1.0 \times 10^9/L$  ( $r = 0.63, p = .04$ ) (Table 3; Fig. 4). We analyzed the delta RSI with a leukocyte count  $>1.0 \times 10^9/L$ . The delta RSI was zero in all 15 ALL children with leukocyte counts  $>1.0 \times 10^9/L$ . The 12 ALL children with a positive delta RSI value all had a low leukocyte count ( $<1.0 \times 10^9/L, n = 36$ ). Therefore, the subset with a leukocyte count  $>1.0 \times 10^9/L$  had a lower ( $p = .01$ ) portion of progressive pneumonia.

### 3.4. Radiological findings of severe cases

The severe and moderate cases were similar when we focused on the individual radiologic signs without RSI scores (Table 4). However, the peak RSI was higher ( $p = .01$ ) in severe cases ( $n = 11$ ) than in moderate cases ( $n = 40$ ). The distribution of peak RSI in severe cases was right-shifted in Fig. 6. A binary logistic analysis found that peak RSI was positively linked with the occurrence of severe pneumonia (OR = 1.15, 95 % CI 1.02–1.29,  $p = .02$ ) when “severe cases” were selected as the “positive outcome”. When compared to delta RSI (AUC: 0.54) or baseline RSI (AUC: 0.68), peak RSI had the widest area under the ROC curve (AUC: 0.76 [0.61, 0.91], optimal cutoff: 4.5) (Fig. 6). Using 4.5 as the cutoff peak, RSI yielded a sensitivity of 73 % and a specificity of 63 % for the severe phenotype of chemotherapy-related pneumonia.

## 4. Discussion

In pediatric oncology practice, chemotherapy-related pneumonia was not uncommon in children with ALL. Our findings indicated that approximately 37 % of all cases among the children receiving first-time chemotherapy were complicated by pneumonia, and 80 % of these children with pneumonia temporarily experienced neutropenia. GGO, an alveolar pathologic sign, appeared in approximately 64 % of all chest CT images. The clinical course of pneumonia was non-progressive in 76 % of cases, with peak RSI equal to the baseline RSI. Those with baseline leukocyte counts  $>1.0 \times 10^9/L$  showed a decreased risk of acquiring progressive pneumonia (delta RSI equal to zero). In severe cases, the peak RSI was higher than that in moderate cases. Peak RSI, with a threshold value of 4.5, a sensitivity of 73 %, and a specificity of 63 %, may predict severe phenotypes owing to respiratory failure.

Our clinical test data were consistent with the UKALL2003 trial (74 % of neutropenic patients and 35 % of infections were respiratory). Our subjects possibly had a higher IRM (a short-term respiratory IRM, 2 %) against the UKALL2003 trial (a 5-year total IRM

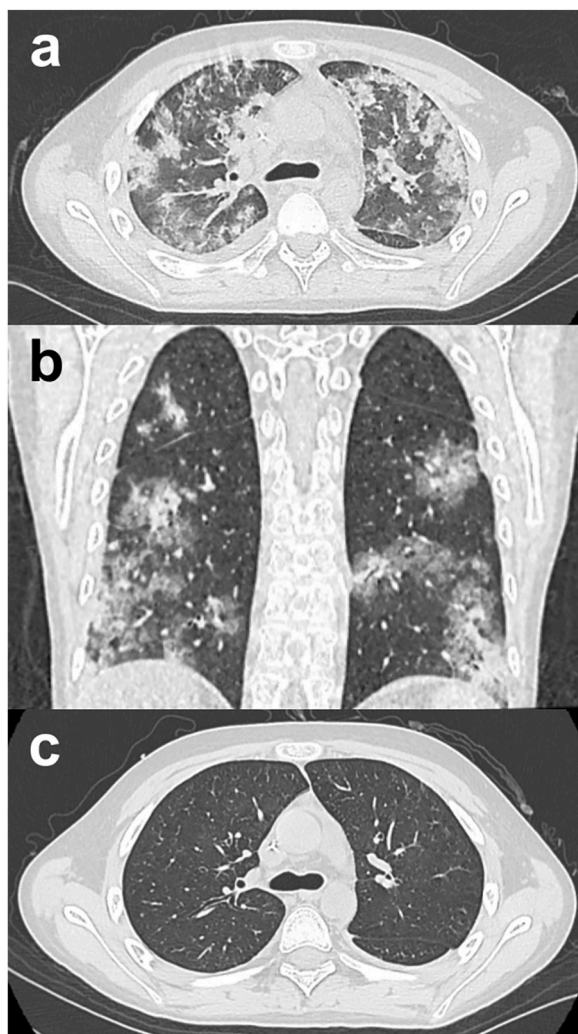


**Fig. 2.** a 13-year-old boy presented fever, a runny nose, and cough during reinduction phase of chemotherapy. The baseline RSI (radiologic severity index) of chest CT was 2 (of 36). The five-day treatment of cephalosporin alone did not improve the symptoms. He developed shortness of breath on the sixth day and the peak RSI of chest CT was 26 (of 36). The BAL (bronchoscopy and bronchoalveolar lavage) was positive of *Pneumocystis jirovecii*. Since then, he was treated in the PICU (pediatric intensive care unit) with respiratory supports, imipenem, vancomycin, and voriconazole. After 10 days of combined treatment of antibacterial and antifungal drugs in the PICU, his lung lesions in CT imaging were absorbed. (a) Axial thin-section unenhanced CT scan shows diffuse bilateral patchy consolidation and ground glass shadows with a peak RSI. (b) Coronal thin-section unenhanced CT image shows bilateral lesions of upper, middle, and lower lung zone. (c) With intensive treatment, the repeated axial CT scan image shows the complete recovery of lung attenuation.

of 2.4 %) [6]. Garcia et al. investigated 716 adult leukemia patients, concluding those who developed pneumonia during chemotherapy (21 %), which was lower than the incidence (36 %) in our study subjects. Adult ALL exhibited a lower incidence (7.1 % [2.3–11.8 %]) of treatment-related pneumonia than adult acute myelogenous leukemia (AML, 21.6 %) and myelodysplastic syndrome (MDS, 29.4 %) [24]. Nevertheless, Sheshadri et al. found that adult ALL with treatment-related pneumonia had higher mortality (10/12) than AML (86/177) and MDS (3/10) [20], all of which being significantly higher than the mortality (1/51, 2 %) in our study subjects. As a result, although chemotherapy-related pneumonia was the most important determinant of early mortality in adult leukemia [24], pneumonia in ALL children showed a lower rate of severe outcome (22 %) and mortality (2 %), based on the findings of the present study.

The radiologic severity score is a practical method to evaluate and trace pulmonary involvement during pneumonia. Using a severity score, a study of SARS-CoV2 infection during the early COVID pandemic dynamically recorded the increasing opacity volume during the 10 days from symptom onset [15]. The semi-quantitative visual evaluation by two experienced radiologists was reliable, and the severity scores correlated with the clinical manifestation. The Ufuk's group also concluded that, with an AUC of 0.816, a cutoff of 6.5 (of 20), a sensitivity of 77 %, and a specificity of 82 %, the semiquantitative score could differentiate between limited and extensive disease status of SARS-CoV2 infection [23]. The Sheshadri group noted that peak RSI could predict mortality of

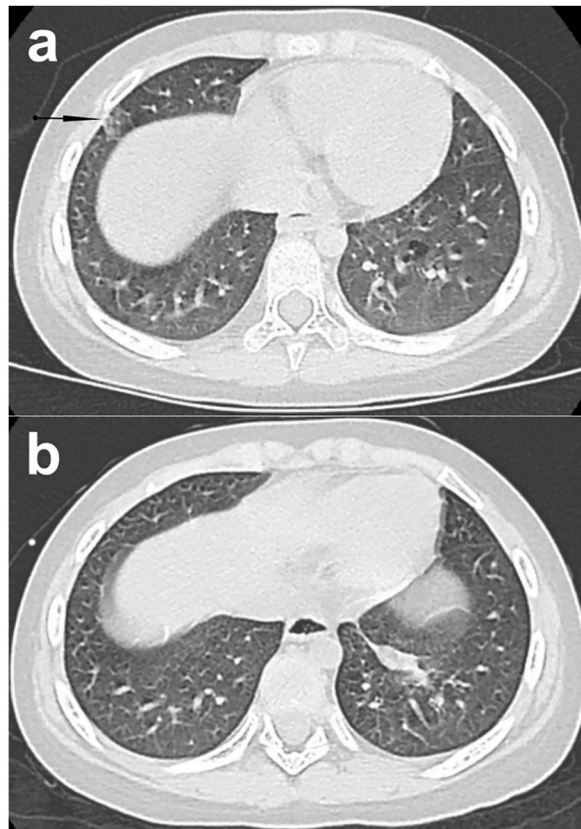


**Fig. 3.** a 4-year-old girl presented fever and cough during induction phase of chemotherapy. The CT imaging confirmed the diagnosis of pneumonia with the baseline RSI (radiologic severity index) of 2 (of 36). Within a 15-day antibacterial treatment, she gradually recovered with a peak RSI of 2 (of 36). (a) Axial thin-section unenhanced CT image shows ground glass opacification (black arrow) in the middle lobe of the right lung with the baseline RSI of 2 (of 36). (b) Her lung lesion was fully absorbed in the axial CT image on the 16th day during pneumonia.

treatment-related pneumonia with an AUC of 0.82, a cutoff of 37.5 (of 72), a sensitivity of 79 %, and a specificity of 71 % [20]. Francone's group concluded that CT parenchymal assessment of SARS-CoV2 lungs may better predict short-term outcomes than non-specific inflammatory biomarkers [19]. Moreover, the direct visualization of anatomic injury and involved volume in CT images could closely relate to the pathological condition. The greater the extent of pulmonary damage (higher RSI score), the higher the possibility of developing hypoxia, which immediately results in death.

Most subjects in our study had relatively lower mortality, as one child (1/51, 2 %) died from complications. Hence, the RSI scores in this study did not relate to mortality. Nonetheless, peak RSI could predict the severe phenotype associated with respiratory failure at cutoff 4.5 (of 36), with optimal sensitivity, specificity, and AUC. Even when hematocyte insufficiency was induced by immunosuppressive treatment, the baseline RSI correlated with the lowest lymphocyte and neutrophil count. Chemotherapy-induced pneumonia did recruit more immune cells in the peripheral blood. The higher the RSI, the more severe the clinical manifestations and immune cell counts. Furthermore, with a relatively higher baseline leukocyte count ( $>1.0 \times 10^9/L$ ), the positive association was more robust, indicating that pneumonia-induced systematic inflammation was more significant, recruited more immune cells, contributed to higher RSIs, and raised CRP levels. Pneumonic children with a higher baseline leukocyte count ( $>1.0 \times 10^9/L$ ) had a lower possibility of developing progressive pneumonia. Therefore, the baseline leukocyte count or the extent of immunosuppression may be a prognostic factor for chemotherapy-related pneumonia.

Due to the complexity of clinical decision-making in diagnosing Community-Acquired Pneumonia (CAP), determining the presence of parenchymal lung disease, which is a crucial factor in pneumonia diagnosis, relies on identifying parenchymal infiltrates on chest X-rays (CXRs) [25]. CXRs offer vital information regarding the location, extent, and associated characteristics of pneumonia [26]. Nevertheless, the significance of radiographic abnormalities remains a subject of debate due to the substantial risk of either missing CAP or overdiagnosing it [27,28]. Agreement among healthcare professionals, regardless of their experience and qualifications, is consistently poor when it comes to identifying parenchymal infiltrates [29,30]. Additionally, the appearance of infiltrates may be delayed, and the accuracy of chest radiographs can be compromised by the presence of coexisting comorbidities [31,32]. CXRs have a sensitivity of 43.5 % and a specificity of 93 % in detecting pulmonary opacities [33]. In the case of CAP, CT scans, considered the gold standard, exhibit sensitivity and specificity levels of 66 % and 77 %, respectively. In studies involving hospitalized CAP patients, CT scans detected up to 35 % of cases missed by initial CXRs [34]. For many patients with COVID-19, CT scans reveal pulmonary infiltrates

**Table 2**  
Chest CT findings of 51 ALL children with chemotherapy-related pneumonia (ALL, acute lymphoblastic leukemia).

Imaging findings	Cases, n = 51 (%)	
	Present	Absent
<b>Pulmonary findings</b>		
Ground-glass shadow	33(64.7)	18(35.3)
Pulmonary opacity/infiltrate	31(60.8)	20(39.2)
Patchy	18(35.3)	33(60.7)
Lobar	4(7.8)	47(92.2)
Funicular	9(17.6)	42(82.4)
Air bronchial sign	5(9.8)	46(90.2)
Nodules	15(29.4)	36(70.6)
< 5 mm	8(15.7)	43(84.3)
5–10 mm	4(7.8)	47(92.2)
> 10 mm	3(5.9)	48(94.1)
Halo sign	6(11.8)	45(88.2)
Air meniscus sign	1(2.0)	50(98.0)
Interlobular septa thickened	5(9.8)	46(90.2)
Central shadow of lobule	2(3.9)	49(96.1)
Bronchiectasis	3(5.9)	48(94.1)
Airway gas retention	3(5.9)	48(94.1)
<b>Intrathoracic non-pulmonary findings</b>		
Pleural effusion	11(21.6)	40(78.4)
Pleural thickening	6(11.8)	45(88.2)
Pericardial effusion	2(3.9)	49(96.1)
Mediastinal displacement	1(2.0)	50(98.0)
lymphadenopathy	6(11.8)	45(88.2)
Bone destruction	3(5.9)	48(94.1)

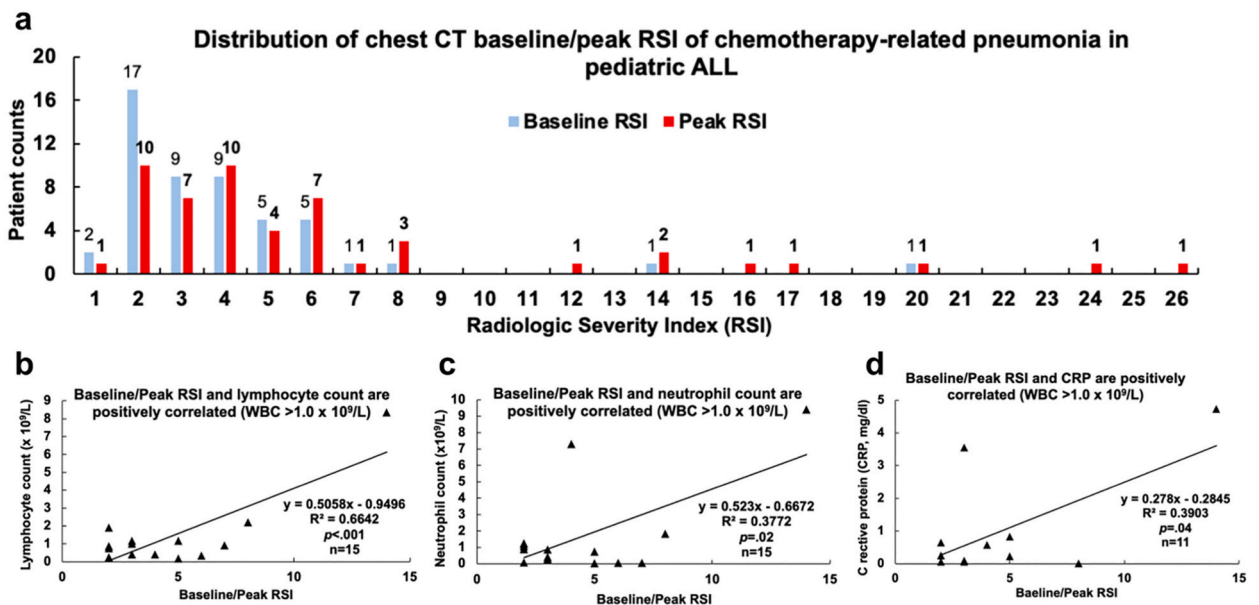


**Fig. 4.** The distribution of the baseline and peak RSI (radiologic severity index) score in the 51 children with chemotherapy-related pneumonia and the correlation between those scores and other clinical features of the children with a baseline leukocyte count over  $1.0 \times 10^9/L$ . (a) The right-skewed distribution of baseline and peak RSI in those 51 ALL children with a maximum peak RSI of 26 (of 36). (b) The baseline/peak RSI score is positively correlated to the lowest lymphocyte count. (c) The baseline/peak RSI score is positively correlated to the lowest neutrophil count. (d) The baseline/peak RSI is positively correlated to the level of C reactive protein. \*Note that those ALL children with a baseline leukocyte count over  $1.0 \times 10^9/L$  experienced non-progressive pneumonia, and hence their baseline RSI score scores were equal to the peak RSI scores respectively. ALL, acute lymphoblastic leukemia; WBC, white blood cell or leukocyte.

not visible on standard CXRs [35]. Therefore, while chest radiographs are commonly used in emergency CAP diagnoses, they are an imperfect gold standard. CT scans are valuable complements to CXRs when radiographic findings are non-specific, when pulmonary complications like empyema or cavitation are present, when there is suspicion of underlying conditions such as lung carcinoma, or

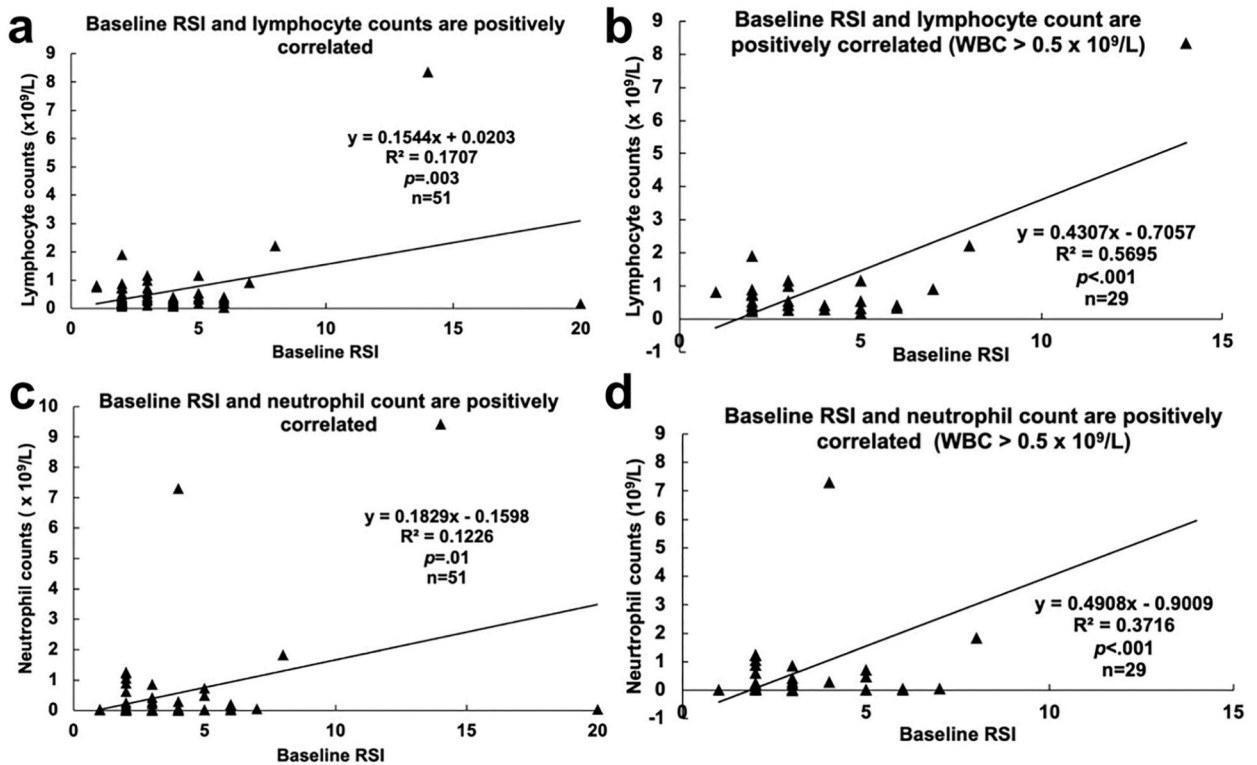


Fig. 5. The baseline RSI (radiologic severity index) is positively correlated with both the lowest lymphocyte and neutrophil counts during chemotherapy-related pneumonia. (a) The baseline RSI and lymphocyte count of the 51 ALL children are positively correlated. (b) The baseline RSI and lymphocyte count are positively correlated in the 29 ALL children with the baseline leukocyte over  $0.5 \times 10^9/L$ . (c) The baseline RSI and neutrophil count of the 51 ALL children are positively correlated. (d) The baseline RSI and neutrophil count are positively correlated in the 29 ALL children with the baseline leukocyte over  $0.5 \times 10^9/L$ . ALL, acute lymphoblastic leukemia; WBC, white blood cell or leukocyte.

Table 3

The baseline RSI had a linear relationship with lymphocyte counts, neutrophil counts, or C reactive protein levels (RSI, radiologic severity index).

with Baseline RSI		Lymphocytes	Neutrophils	C reactive protein
WBC>0	r	0.413 <sup>a</sup>	0.350 <sup>b</sup>	0.221
n = 51	p	0.003	0.01	0.17 (n = 40)
WBC>0.5	r	0.755 <sup>a</sup>	0.610 <sup>a</sup>	0.465 <sup>b</sup>
n = 29	p	<0.001	<0.001	0.03 (n = 23)
WBC>1.0	r	0.815 <sup>a</sup>	0.614 <sup>a</sup>	0.625 <sup>b</sup>
n = 15	p	<0.001	<0.001	0.04 (n = 11)

<sup>a</sup> At the 0.01 level (two-tailed), the association was significant.

<sup>b</sup> At the 0.05 level (two-tailed), the association was significant.

when pneumonia is recurrent or non-resolving [36]. Although this supportive role of CT scans is presumed to apply to hospital-acquired pneumonia (HAP) patients, conclusive evidence is lacking. Overall, CT scans enhance practitioner confidence in CAP diagnosis. They offer a better assessment of lung involvement (detecting multifocal or bilateral localization), identifying complications, and approximating pathological changes.

It's worth noting that recommendations for daily practice are primarily based on standard radiographs, despite the improvement in CAP diagnosis through CT scans [25]. The adaptation and variation of treatment based on CT scan results remain a topic of debate. Studies have indicated that initiating antibiotics in patients diagnosed with CAP via CT scan may positively impact their prognosis [34]. The crucial concern is the increased radiation exposure associated with CT scans. In our study, the median CTDIvol (DLP) measured 2.57 mGy (60.01 mGy cm), roughly equivalent to the annual natural radiation dose received by an average person. Furthermore, advancements in reconstruction techniques have brought CT scan radiation levels down to those of standard chest X-rays, ensuring satisfactory quality for meaningful studies [37].

Lung ultrasonography is now a common imaging method in emergency departments and intensive care units (ICUs). Its advantages over CT scans include no radiation exposure, bedside accessibility, and reasonable diagnostic accuracy [38]. However, mastering this technique can be challenging, particularly in mechanically ventilated patients. A systematic review revealed lung ultrasonography's

**Table 4**  
Chest CT image findings of severe cases and moderate cases and comparison.

Imaging findings	Patients, No.(%)		p value
	Severe cases	Moderate cases	
<b>Pulmonary findings</b>			
ground-glass shadow			
Yes	8	25	.726
No	3	15	
pulmonary opacity/infiltrate			
Yes	6	25	.732
No	5	15	
nodules			
Yes	3	12	1.000
No	8	28	
Interstitial involvement			
Yes	3	4	.162
No	8	36	
bronchiectasis			
Yes	1	2	.526
No	10	38	
<b>Intrathoracic non-pulmonary findings</b>			
Pleural effusion			
Yes	3	8	.684
No	8	32	
Pleural thickening			
Yes	0	6	.319
No	11	34	
Pericardial effusion			
Yes	1	1	.388
No	10	39	
lymphadenopathy			
Yes	1	5	1.00
No	10	35	
Bone destruction			
Yes	1	2	.526
No	10	38	
<b>RSI</b>			
Baseline RSI	4(3–6)	3(2–4)	.057
Peak RSI	6(4–16)	4(2–6)	.009
Delta RSI	0(0–6)	0(0–0)	.590
RSI varying-rate	0(0–0.361)	0(0–0)	.633

Data are n(%) and median (interquartile range). RSI, Radiologic Severity Index.

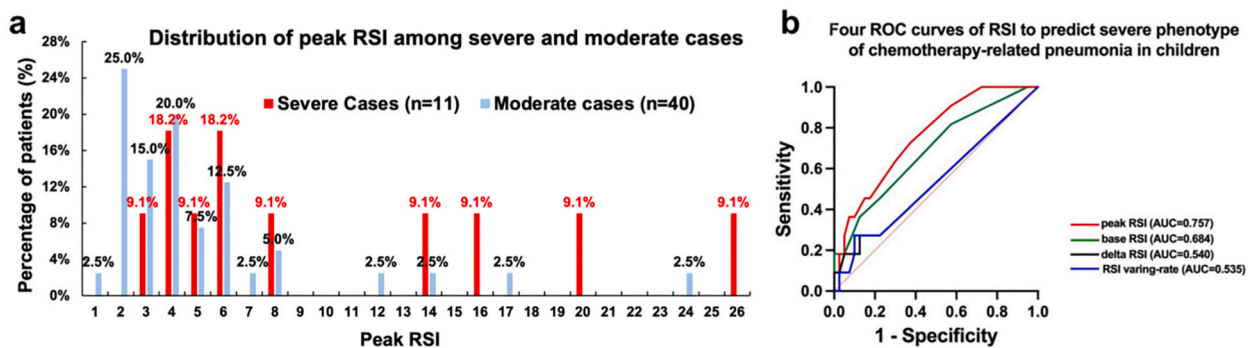


**Fig. 6.** The peak RSI (radiologic severity index) scores of severe cases (n = 11) are higher than moderate cases and able to predict the severe phenotype. (a) The distribution of peak RSI scores of severe and moderate cases. The distribution of severe cases' score is right-shifted compared with moderate cases. (b) ROC (receiver operating characteristic) curves of baseline RSI (yellow), peak RSI (red), delta RSI (black) and RSI varying-rate (blue). Peak RSI has the best diagnostic performance to predict the severe cases (clinically associated with respiratory failure) with AUC of 0.76 ([0.61, 0.91], optimal cutoff: 4.5). AUC, area under the curve.

sensitivity at 88 % and specificity at 89 %, with a 90 % probability of accurately diagnosing pneumonia [39]. Diagnosing ventilation-associated pneumonia (VAP) through echography is more intricate, and only a limited number of observational studies have addressed this thus far [39].

This study was retrospective and single-centered. We may have some biased results due to the small sample size. The children participating in the research with chemotherapy-related pneumonia were of Chinese ethnicity, and the results may not be representative of other ethnic groups. The visual assessment of CT images could have been semi-quantitative and less precise than the quantitative methods such as the digit image viewer [40].

In conclusion, chest CT images with radiologic severity scores that clinically correlated with lymphocyte/neutrophil counts, inflammatory markers, and predicted severe phenotypes may be used to evaluate chemotherapy-related pneumonia in children. This study could draw the attention of researchers and oncologists to treatment-related toxicity, particularly in a pediatric population with hematologic malignancies.

## Funding

This work was supported by the Sanming Project of Medicine in Shenzhen (NO. SZSM202011005), High-level Hospital Construction Project of Guangdong (NO. ynk2021-zz13) and Natural Science Foundation of Shenzhen City (NO. JCYJ20220530155607018).

## Data availability statement

We ensure that data is available, and that research-related data is stored in publicly available repositories (10.17632/z23yhsxw5m.1).

## Ethics declarations

Our study was approved by the Research Ethics Committee of Shenzhen Children's Hospital, China (Protocol number JCYJ20220530155607018). Informed consent is not required for this study because the protocol is retrospective. We determined that our study complied with all regulations.

## CRedit authorship contribution statement

**Zhixin Gao:** Writing – review & editing, Writing – original draft, Software, Resources, Methodology, Formal analysis, Data curation. **Ke Wei:** Writing – review & editing, Methodology. **Ruiyuan Chen:** Writing – original draft, Resources. **Wenhong Ye:** Writing – review & editing, Investigation, Conceptualization. **Tian Li:** Writing – review & editing, Visualization, Software, Methodology. **Qiru Su:** Visualization, Software, Methodology. **Rong Wang:** Writing – review & editing, Project administration, Conceptualization. **Weiguo Cao:** Writing – review & editing, Supervision, Investigation, Funding acquisition, Conceptualization.

## Declaration of competing interest

The authors declare that they have no known competing financial interests or personal relationships that could have appeared to influence the work reported in this paper.

## References

- [1] S.P. Hunger, C.G. Mullighan, Acute lymphoblastic leukemia in children, *N. Engl. J. Med.* 373 (2015) 1541–1552, <https://doi.org/10.1056/NEJMra1400972>.
- [2] D. Siegel, J. Li, S.J. Henley, R. Wilson, N.B. Lunsford, E. Tai, et al., Incidence rates and trends of pediatric cancer - United States, 2001-2014, *Pediatr. Blood Cancer* 65 (2018), <https://doi.org/10.15585/mmwr.mm6636a3>.
- [3] A. Moricke, A. Reiter, M. Zimmermann, H. Gadner, M. Stanulla, M. Dordelmann, et al., Risk-adjusted therapy of acute lymphoblastic leukemia can decrease treatment burden and improve survival: treatment results of 2169 unselected pediatric and adolescent patients enrolled in the trial ALL-BFM 95, *Blood* 111 (2008) 4477–4489, <https://doi.org/10.1182/blood-2007-09-112920>.
- [4] H. Inaba, D. Pei, J. Wolf, S.C. Howard, R.T. Hayden, M. Go, et al., Infection-related complications during treatment for childhood acute lymphoblastic leukemia, *Ann. Oncol.* 28 (2017) 386–392, <https://doi.org/10.1093/annonc/mdw557>.
- [5] M.S. Christensen, M. Heyman, M. Mottonen, B. Zeller, G. Jonmundsson, H. Hasle, et al., Treatment-related death in childhood acute lymphoblastic leukaemia in the Nordic countries: 1992-2001, *Br. J. Haematol.* 131 (2005) 50–58, <https://doi.org/10.1111/j.1365-2141.2005.05736.x>.
- [6] D. O'Connor, J. Bate, R. Wade, R. Clack, S. Dhir, R. Hough, et al., Infection-related mortality in children with acute lymphoblastic leukemia: an analysis of infectious deaths on UKALL2003, *Blood* 124 (2014) 1056–1061, <https://doi.org/10.1182/blood-2014-03-560847>.
- [7] D. Hasegawa, T. Imamura, K. Yumura-Yagi, Y. Takahashi, I. Usami, S. Suenobu, et al., Risk-adjusted therapy for pediatric non-T cell ALL improves outcomes for standard risk patients: results of JACLS ALL-02, *Blood Cancer J.* 10 (2020). ARTN 23 10.1038/s41408-020-0287-4.
- [8] B. Lund, A. Asberg, M. Heyman, J. Kanerva, A. Harila-Saari, H. Hasle, et al., Risk factors for treatment related mortality in childhood acute lymphoblastic leukaemia, *Pediatr. Blood Cancer* 56 (2011) 551–559, <https://doi.org/10.1002/psc.22719>.
- [9] T. Oskarsson, S. Soderhall, J. Arvidson, E. Forestier, T.L. Frandsen, M. Hellebostad, et al., Treatment-related mortality in relapsed childhood acute lymphoblastic leukemia, *Pediatr. Blood Cancer* 65 (2018), <https://doi.org/10.1002/psc.26909>.
- [10] J. Torres-Flores, R. Espinoza-Zamora, J. Garcia-Mendez, E. Cervera-Ceballos, A. Sosa-Espinoza, N. Zapata-Canto, Treatment-related mortality from infectious complications in an acute leukemia clinic, *J. Hematol.* 9 (2020) 123–131, <https://doi.org/10.14740/jh751>.
- [11] C. Orasch, M. Weisser, D. Mertz, A. Conen, D. Heim, S. Christen, et al., Comparison of infectious complications during induction/consolidation chemotherapy versus allogeneic hematopoietic stem cell transplantation, *Bone Marrow Transplant.* 45 (2010) 521–526, <https://doi.org/10.1038/bmt.2009.187>.
- [12] C. Gudiol, C. Royo-Cebrecos, J. Laporte, C. Ardanuy, C. Garcia-Vidal, M. Antonio, et al., Clinical features, aetiology and outcome of bacteraemic pneumonia in neutropenic cancer patients, *Respirology* 21 (2016) 1411–1418, <https://doi.org/10.1164/rccm.201501-0017OC>.
- [13] R. Eibel, P. Herzog, O. Dietrich, C.T. Rieger, H. Ostermann, M.F. Reiser, et al., Pulmonary abnormalities in immunocompromised patients: comparative detection with parallel acquisition MR imaging and thin-section helical CT, *Radiology* 241 (2006) 880–891, <https://doi.org/10.1148/radiol.2413042056>.

- [14] Y.E. Claessens, M.P. Debray, F. Tubach, A.L. Brun, B. Rammaert, P. Hausfater, et al., Early chest computed tomography scan to assist diagnosis and guide treatment decision for suspected community-acquired pneumonia, *Am. J. Respir. Crit. Care Med.* 192 (2015) 974–982, <https://doi.org/10.1164/rccm.201501-0017OC>.
- [15] P. Feng, Y. Tianhe, S. Peng, G. Shan, L. Bo, L. Lingli, et al., Time course of lung changes at chest CT during recovery from coronavirus disease 2019 (COVID-19), *Radiology* 295 (3) (2020) 715–721, <https://doi.org/10.1148/radiol.2020200370>.
- [16] M. Chung, A. Bernheim, X. Mei, N. Zhang, M. Huang, X. Zeng, et al., CT imaging features of 2019 novel coronavirus (2019-nCoV), *Radiology* 295 (2020) 202–207, <https://doi.org/10.1148/radiol.2020200230>.
- [17] S. Sharma, A. Aggarwal, R.K. Sharma, E. Patras, A. Singhal, Correlation of chest CT severity score with clinical parameters in COVID-19 pulmonary disease in a tertiary care hospital in Delhi during the pandemic period, *Egyptian Journal of Radiology and Nuclear Medicine* 53 (2022), <https://doi.org/10.1186/s43055-022-00832-x>.
- [18] F. Feng, Y. Jiang, M. Yuan, J. Shen, H. Yin, D. Geng, et al., Association of radiologic findings with mortality in patients with avian influenza H7N9 pneumonia, *PLoS One* 9 (2014), e93885, <https://doi.org/10.1371/journal.pone.0093885>.
- [19] M. Francone, F. Iafraite, G.M. Masci, S. Coco, F. Cilia, L. Manganaro, et al., Chest CT score in COVID-19 patients: correlation with disease severity and short-term prognosis, *Eur. Radiol.* 30 (2020) 6808–6817, <https://doi.org/10.1007/s00330-020-07033-y>.
- [20] A. Sheshadri, M. Godoy, J.J. Erasmus, S. Gruschkus, A. Hasan, S.E. Evans, et al., Progression of the Radiologic Severity Index is associated with increased mortality and healthcare resource utilisation in acute leukaemia patients with pneumonia, *BMJ Open Respir Res* 6 (2019), e000471, <https://doi.org/10.1136/bmjresp-2019-000471>.
- [21] D.M. Hansell, A.A. Bankier, H. MacMahon, T.C. McLoud, N.L. Muller, J. Remy, Fleischner Society: glossary of terms for thoracic imaging, *Radiology* 246 (2008) 697–722, <https://doi.org/10.1148/radiol.2462070712>.
- [22] S.W. Lee, S.H. Park, K.W. Kim, E.K. Choi, Y.M. Shin, P.N. Kim, et al., Unenhanced CT for assessment of macrovesicular hepatic steatosis in living liver donors: comparison of visual grading with liver attenuation index, *Radiol.* 244 (2) (2007 Aug) 479–485, <https://doi.org/10.1148/radiol.2442061177>.
- [23] H.J. Park, K.W. Kim, H.J. Kwon, S. Lee, D.W. Kim, H.H. Moon, et al., CT-based visual grading system for assessment of hepatic steatosis: diagnostic performance and interobserver agreement, *Hepatol Int* 16 (5) (2022 Oct) 1075–1084, <https://doi.org/10.1007/s12072-022-10373-0>.
- [24] J.B. Garcia, X. Lei, W. Wierda, J.E. Cortes, B.F. Dickey, S.E. Evans, et al., Pneumonia during remission induction chemotherapy in patients with acute leukemia, *Ann Am Thorac Soc* 10 (2013) 432–440, <https://doi.org/10.1513/AnnalsATS.201304-097OC>.
- [25] Z. Kanjee, J.P. Metlay, A. Moskowitz, E.E. Reynolds, How would you treat this patient hospitalized with community-acquired pneumonia? *Ann. Intern. Med.* 174 (12) (2021) 1719–1726, <https://doi.org/10.7326/M21-3650>.
- [26] J.P. Metlay, G.W. Waterer, A.C. Long, A. Anzueta, J. Brozcek, K. Crothers, et al., Diagnosis and treatment of adults with community-acquired pneumonia. An official clinical practice guideline of the American thoracic society and infectious diseases society of America, *Am. J. Respir. Crit. Care Med.* 200 (7) (2019) e45–e67, <https://doi.org/10.1164/rccm.201908-1581ST>.
- [27] M. Young, T.J. Marrie, Interobserver variability in the interpretation of chest roentgenograms of patients with possible pneumonia, *Arch. Intern. Med.* 154 (23) (1994) 2729, <https://doi.org/10.1001/archinte.1994.00420230122014>.
- [28] F.M. de Benedictis, E. Kerem, A.B. Chang, A.A. Colin, H.J. Zar, A. Bush, Complicated pneumonia in children, *Lancet* 396 (10253) (2020 Sep 12) 786–798, [https://doi.org/10.1016/S0140-6736\(20\)31550-6](https://doi.org/10.1016/S0140-6736(20)31550-6).
- [29] V. Novack, L.S. Avnon, A. Smolyakov, R. Barnea, A. Jotkowitz, F. Schlaeffer, Disagreement in the interpretation of chest radiographs among specialists and clinical outcomes of patients hospitalized with suspected pneumonia, *Eur. J. Intern. Med.* 17 (1) (2006 Jan) 43–47, <https://doi.org/10.1016/j.ejim.2005.07.008>.
- [30] M.N. Albaum, L.C. Hill, M. Murphy, Y.H. Li, C.R. Fuhrman, C.A. Britton, et al., Interobserver reliability of the chest radiograph in community-acquired pneumonia. PORT Investigators, *Chest* 110 (2) (1996 Aug) 343–350, <https://doi.org/10.1378/chest.110.2.343>.
- [31] J. Rello, R. Rodriguez, P. Jubert, B. Alvarez, Severe community-acquired pneumonia in the elderly: epidemiology and prognosis. Study Group for Severe Community-Acquired Pneumonia, *Clin. Infect. Dis.* 23 (4) (1996 Oct) 723–728, <https://doi.org/10.1093/clinids/23.4.723>.
- [32] V.F. Corrales-Medina, D.M. Musher, G.A. Wells, J.A. Chirinos, L. Chen, M.J. Fine, Cardiac complications in patients with community-acquired pneumonia: incidence, timing, risk factors, and association with short-term mortality, *Circulation* 125 (6) (2012 Feb 14) 773–781, <https://doi.org/10.1161/CIRCULATIONAHA.111.040766>.
- [33] W.H. Self, D.M. Courtney, C.D. McNaughton, R.G. Wunderink, J.A. Kline, High discordance of chest x-ray and computed tomography for detection of pulmonary opacities in ED patients: implications for diagnosing pneumonia, *Am. J. Emerg. Med.* 31 (2) (2013 Feb) 401–405, <https://doi.org/10.1016/j.ajem.2012.08.041>.
- [34] Y.E. Claessens, M.P. Debray, F. Tubach, A.L. Brun, B. Rammaert, P. Hausfater, et al., Early chest computed tomography scan to assist diagnosis and guide treatment decision for suspected community-acquired pneumonia, *Am. J. Respir. Crit. Care Med.* 192 (8) (2015 Oct 15) 974–982, <https://doi.org/10.1164/rccm.201501-0017OC>.
- [35] X. Ding, J. Xu, J. Zhou, Q. Long, Chest CT findings of COVID-19 pneumonia by duration of symptoms, *Eur. J. Radiol.* 127 (2020 Jun), 109009, <https://doi.org/10.1016/j.ejrad.2020.109009>. Epub 2020 Apr 18.
- [36] T. Franquet, Imaging of community-acquired pneumonia, *J. Thorac. Imag.* 33 (5) (2018 Sep) 282–294, <https://doi.org/10.1097/RTI.0000000000000347>.
- [37] K.B. Mathieu, H. Ai, P.S. Fox, M.C. Godoy, R.F. Munden, P.M. de Groot, et al., Radiation dose reduction for CT lung cancer screening using ASIR and MBIR: a phantom study, *J. Appl. Clin. Med. Phys.* 15 (2) (2014 Mar 6) 4515, <https://doi.org/10.1120/jacmp.v15i2.4515>.
- [38] M. D'Amato, G. Rea, V. Carnevale, M.A. Grimaldi, A.R. Saponara, E. Rosenthal, et al., Assessment of thoracic ultrasound in complementary diagnosis and in follow up of community-acquired pneumonia (cap), *BMC Med. Imag.* 17 (1) (2017 Aug 31) 52, <https://doi.org/10.1186/s12880-017-0225-5>.
- [39] M.A. Chavez, N. Shams, L.E. Ellington, N. Naithani, R.H. Gilman, M.C. Steinhoff, et al., Lung ultrasound for the diagnosis of pneumonia in adults: a systematic review and meta-analysis, *Respir. Res.* 15 (1) (2014 Apr 23) 50, <https://doi.org/10.1186/1465-9921-15-50>.
- [40] F. Ufuk, M. Demirci, E. Ugurlu, N. Cetin, N. Yigit, T. Sari, Evaluation of disease severity with quantitative chest CT in COVID-19 patients, *Diagn Interv Radiol* 27 (2021) 164–171, <https://doi.org/10.5152/dir.2020.20281>.